This paper describes objective technical results and analysis. Any subjective views or opinions that might be expressed in the paper do not necessarily represent the views of the U.S. Department of Energy or the United States Government.

SAND2022-5335C

Data-driven Modeling of Commercial Photovoltaic Inverter Dynamics Using Power Hardware-in-the-Loop

Nischal Guruwacharya[†1], Harish Bhandari[1], Sunil Subedi[1], Jesus D. Vasquez-Plaza[2], Matthew Lee Stoel[3], Ujjwol Tamrakar[4], Felipe Wilches-Bernal[4], Fabio Andrade[2], Timothy M. Hansen[1], and Reinaldo Tonkoski[1]

***Abstract*—Grid technologies connected via power electronic converter (PEC) interfaces increasingly include the grid support functions for voltage and frequency support defined by the IEEE 1547-2018 standard. The shift towards converter-based generation necessitates accurate PEC models for assessing system dynamics that were previously ignored in conventional power systems. In this paper, a method for assessing photovoltaic (PV) inverter dynamics using a data-driven technique with power hardware-in-the-loop is presented. The data-driven modeling technique uses various probing signals to estimate commercial off-the-shelf (COTS) inverter dynamics. The MATLAB system identification toolbox is used to develop a dynamic COTS inverter model from the perturbed grid voltage (i.e., probing signal) and measured current injected to the grid by the inverter. The goodness-of-fit of COTS inverter dynamics in Volt-VAr support mode under each probing signal is compared. The results show that the logarithmic square-chirp probing signal adequately excites the COTS inverter in Volt-VAr mode to fit a data-driven dynamic model.**

***Index Terms*—Data-driven modeling, grid support functions, power hardware-in-the-loop, real-time digital simulator, system identification.**

I. Introduction

Over the last decade, the share of renewable energy in global electricity generation has increased steadily and is projected to reach 67.3% by 2040 [1]. As most renewable energy sources interface with the grid via power electronic converters (PECs), they are increasingly impacting power system dynamics. Through new standards, PECs are required to support grid voltage and frequency via grid support functions (GSFs), which are implemented in a variety of ways depending on the manufacturer even under the same operating conditions [2], [3]. Moreover, the detailed architecture of inverters and their controls are proprietary and are not known. This can lead to improper modeling and simulation of power systems and affect the dynamics of PECs, resulting in inaccurate results and analysis. Hence, a method is required to design a general, efficient dynamic model extraction technique for PEC with GSFs.

Various modeling approaches are available in the literature that aims to capture the PEC dynamics accurately. Switched models are considered the most detailed approach that captures the overall non-linear dynamics. However, they are computationally intractable for dynamic analysis of large power systems [4]. Averaged linear models reduce the computational cost by neglecting the effect of switching dynamics [5], [6]. Dynamic phasor models can be more accurate than the average model but are mathematically complex [7]. On the other hand, data-driven system identification (SysId) approaches generate PEC models from experimental data that do not demand the system details. Thus, it could be used to resolve the aforementioned problem [8], [9]. In data-driven modeling, perturbing the PECs with correctly designed probing signals plays a vital role. The probing signals used have a significant impact on the data that is measured and allow for accurate estimation of system parameters and identification of linear transfer functions (TFs) to capture the PV inverter dynamics [10]. In [11], accurately identified power system linear dynamics with sinusoidal and exponential chirp probing signals is presented, but the impact in GSFs inverter when obtaining the linear models of power systems has not been considered.

The main objective of this paper is to design a data-driven modeling approach for extracting the PV inverter dynamics utilizing various probing signals (square, sine, square-chirp, and sine-chirp). A dynamic model of a commercial off-the-shelf (COTS) inverter is obtained using the SysId toolbox available in MATLAB and is validated under the Volt-VAr GSF. Furthermore, the study analyzes the goodness-of-fit (GoF) when the COTS inverter is perturbed with probing

[1] South Dakota State University, Electrical Engineering and Computer Science Department, Brookings, SD, USA. [†] corresponding author: nischal.guruwacharya@jacks.sdstate.edu

[2] University of Puerto Rico Mayaguez, Electrical Engineering and Computer Science Department, Puerto Rico, USA.

[3] Ulteig Engineers, Sioux Falls, SD, USA.

[4] Sandia National Laboratories, Albuquerque, NM, USA.

This work is supported by the U.S. Department of Energy Office of Science, Office of Basic Energy Sciences, EPSCoR Program; and Office of Energy Efficiency and Renewable Energy, Solar Energy Technology Office under EPSCoR grant number DE-SC0020281. This work made use of the Opal-RT real-time simulator purchased as part of the National Science Foundation (NSF) grant number MRI-1726964. The work at Sandia (Ujjwol Tamrakar) is supported by the US Department of Energy, Office of Electricity, Energy Storage Program.

Sandia National Laboratories is a multi-mission laboratory managed and operated by National Technology and Engineering Solutions of Sandia, LLC., a wholly owned subsidiary of Honeywell International, Inc., for the U.S. Department of Energy National Nuclear Security Administration under contract DE-NA-0003525. This paper describes objective technical results and analysis. Any subjective views or opinions that might be expressed in the paper do not necessarily represent the views of the U.S. Department of Energy or the United States Government.

Sandia National Laboratories is a multimission laboratory managed and operated by National Technology & Engineering Solutions of Sandia, LLC, a wholly owned subsidiary of Honeywell International Inc., for the U.S. Department of Energy's National Nuclear Security Administration under contract DE-NA0003525.

signals and indicates which one would estimate an accurate PV inverter model.

The rest of the paper is organized as follows. Section II presents a method to assess PV inverter dynamics with GSFs. Different probing signals used in the paper are discussed followed by partitioned modeling of Volt-VAr. Section III presents the experimental setup for identifying the TF of the COTS inverter (Fronius Symo Inverter) using different probing signals and the results are presented in Section IV. Finally, Section V concludes the study.

II. Modeling COTS Inverter Dynamics with GSFs

In this section, the basic concept of SysId to obtain the accurate COTS inverter dynamics model is explained. Then, the various probing signals are explained, and the partitioned modeling is described to capture the non-linear dynamics of the PV inverter operating in Volt-VAr mode, followed by the flowchart to assess the TF of the inverter.

A. System Identification of PEC

SysId is the process of obtaining a mathematical model of an unknown system based on input and its corresponding output data. Without knowing the actual control structure and/or control parameters, a mathematical model of a PEC that captures the dynamics of interest can be estimated by using Instrument variable method. The basic concept of a SysId process is illustrated in Fig. 1. The time domain input data $u(t)$ and time domain output data $y(t)$ from the unknown dynamic systems to be identified are first measured. The dataset is then divided into training and testing datasets. The training dataset is passed into a SysId toolbox (implemented in MATLAB), which estimates the system parameters (i.e. coefficient of TF) by minimizing a defined cost function (least-square error). From the estimated parameters, a TF is obtained [8]. The testing dataset is then used to validate the TF obtained. Finally, GoF based on normalized root-mean-square-error (NRMSE) is calculated to check the accuracy of the TF.

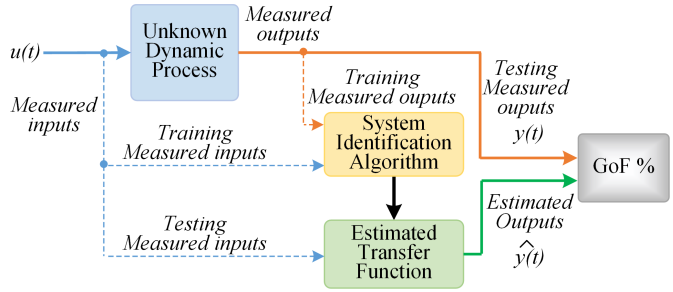

Fig. 1. The fundamental concept of SysId. To identify the unknown dynamic process, the SysId method utilizes input and output measurements. The GoF is then calculated by comparing the actual outputs and estimated outputs.

B. Probing Signals

This paper examines the impact of the square wave (Sq), sine wave (Sine), logarithmic square chirp (Sq-Chirp), and logarithmic sine chirp (Sine-Chirp) signals on the derived linear models of different regions for Volt-VAr mode of operation. The selected signals used in the test are designed from the standpoint of SysId theory, as well as design restrictions imposed by the power system. SysId theory states that the spectrum of the probing signal determines the validity of the estimated parameters and the main concept of identification theory is to position the content of the probing signal in the frequency band of interest by the application [10].

C. Partitioned Modeling of Volt-VAr

According to IEEE 1547-2018 standard [12], the Volt-VAr mode of operation is activated when a distributed energy resource is actively required to support the grid voltage. When the grid voltage falls below the deadband range, the inverter injects reactive power (+VAr) into the grid. Likewise, when the grid voltage increases above the deadband range, the inverter absorbs reactive power (-VAr) from the grid. Finally, within the deadband, the inverter does not inject nor absorb reactive power. The piecewise linear Volt-VAr characteristics consist of voltage parameters (V_1, V_2, V_3, and V_4) and reactive power parameters (Q_1, Q_2, Q_3, and Q_4) which are configured as specified in the updated IEEE 1547-2018 standard. Due to the presence of nonlinearities in PECs, modeling of PECs with GSFs over diverse operating regions results in intricate dynamic models, and the complex dynamics of the whole operating region are not effectively captured by a single linearized model [13]. Therefore, the inverter operating regions are further divided into multiple linear regions. Each region (represented by R) is separated into several small ranges (represented by r) based on the magnitude of voltage. A linear transfer function for each range is determined using the SysId toolbox available in MATLAB and can be combined by a suitable mechanism [14]. Several regions and ranges of the Volt-VAr characteristics curve are shown in Fig. 2, where $r_{11}, r_{12}, .., r_{21}, r_{22}, .., r_{5k}$ are ranges; the first index represents the region and second index represents voltage amplitude change.

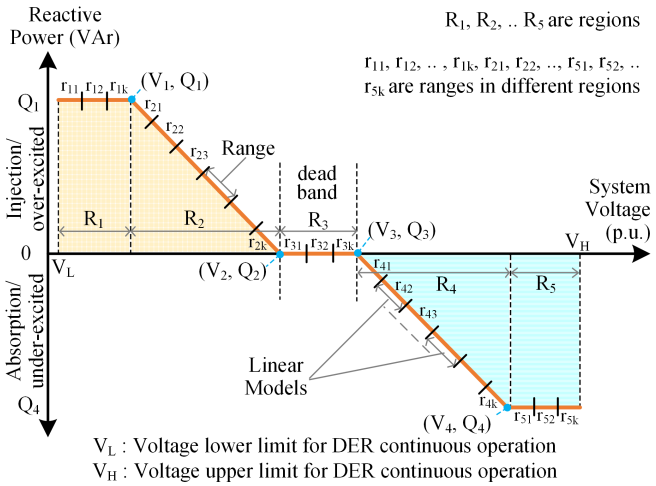

Fig. 2. The Volt-VAr characteristics curve depicts several regions and ranges.

D. Flowchart to Assess COTS Inverter Dynamics

The flowchart to identify the TF of a COTS inverter operating in Volt-VAr mode from the SysId algorithm is shown in Fig. 3. Different probing signals of varying voltage amplitude were used to perturb the COTS inverter. The parameters for the probing signals used are shown in Table I. For all probing signals, voltage amplitude is varied from 0.895 p.u. to 0.905 p.u. for 15 sec and then the amplitude is increased by 0.005 p.u. for the next range until amplitude reached 1.095 p.u. Here, 0.01 p.u. step-change is done based on the region 5 voltage range availability on Volt-VAr mode. The frequency for Sine and Sq wave is 1 Hz and that for Sine-Chirp and Sq-Chirp is varied from 1 Hz to 32 Hz. The values of frequency are chosen based on the settling time response parameters of the COTS inverter.

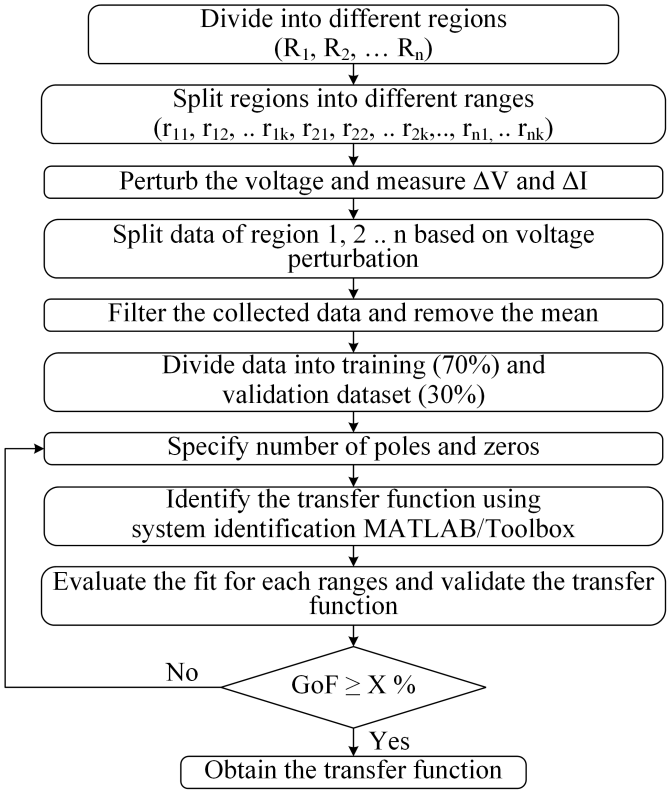

Fig. 3. Flowchart to identify TF using SysId algorithm.

TABLE I
Parameters of probing signals.

Input Signal	Voltage Amplitude Variation (p.u.)	Step Change (p.u.)	Frequency (Hz)
Sine	0.895-1.095	0.01	1
Sq	0.895-1.095	0.01	1
Sine-Chirp	0.895-1.095	0.01	1-32
Sq-Chirp	0.895-1.095	0.01	1-32

To identify the TF of each range, voltage amplitude (measured inputs) at the point-of-common-coupling (PCC) and current injected by the COTS inverter to the grid (measured outputs) are logged through the Opal-RT system, and thus, collected data are split into different regions. Then, the data is filtered using the mean filter to smooth the array of sampled data. Furthermore, the mean of both voltage and current measurements are eliminated to obtain a more accurate model. This allows SysId to focus on the real variations caused by the probing signals rather than undesirable data trends. The dataset is separated into two parts for cross-validation: a training set for computing unknown poles and zeros, and a validation set for validating the resulting model. Then, the poles and zeroes are swept from a second-order to a fifth-order model to generate distinct linearized models that are accurate and computationally efficient, using a SysId technique. i_q current from the inverter ($y(t)$) and from the TF models ($\hat{y}(t)$) are used to calculate GoF based on NRMSE as in Eq. 1 and is defined as [15]:

$$\text{GoF} = 100 \times \left(1 - \frac{\|y(t) - \hat{y}(t)\|_2}{\|y(t) - \text{mean } y(t)\|_2}\right) \quad (1)$$

where, $\|.\|_2$ indicates 2-norm vector.

Moreover, models with respective poles and zeroes are compared using the Akaike's Final Prediction Error (AFPE) and the most accurate model with the lowest AFPE is chosen as the final TF model for each range [8]. Aggregating all selected TFs will replicate inverter dynamics for the entire operating region.

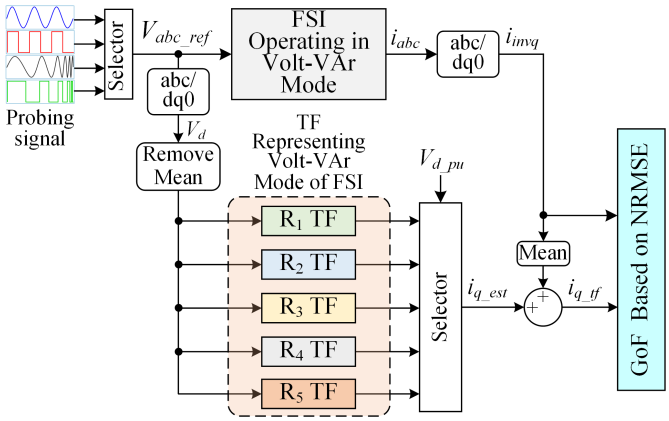

Fig. 4. Schematic diagram to validate the TF obtained from SysId when COTS inverter is operating in Volt-VAr mode.

Fig. 4 depicts a schematic diagram to validate the TF acquired via SysId. To validate the accuracy of the TFs, the COTS inverter was excited through the Puissance Plus Power Amplifier with the same probing signal in parallel with its TFs. V_{abc_ref} is the reference voltage amplitude at PCC. The output current injected to the power amplifier by the COTS inverter was passed to $abc - dq0$ block to only obtain quadrature axis current, i_{invq} because the COTS inverter was operated in Volt-VAr mode. The power amplifier was used to produce different probing signals as explained in Section II-B and changes in voltage amplitude of the probing signals were applied to the COTS inverter as shown in the experimental setup of Fig. 5 to capture the dynamics of the inverter. Here, V_{abc_ref} was

converted to $dq0$ component, and only the d-component (V_d) was used as it is associated with the voltage amplitude. The mean value of V_d was removed before feeding to the TF of different regions. The output of the TF was the estimated current which was inputted to the selector block. The selector block chose the correct estimated current based on the per-unit value of voltage V_{d_pu}. Mean value of sensed current (i_{invq}) was then added in the estimated current (i_{q_est}) to get actual estimated current (i_{q_tf}) from the TF block. The GoF based on NRMSE was then calculated to compare the fit percent.

III. Experimental Setup

A power hardware-in-the-loop (PHIL) arrangement can be used to test COTS inverters in a variety of voltage and frequency conditions. Here, the equipment under test is a commercial three-phase 10 kW Fronius Symo Inverter (FSI) whose TF model is to be determined when it is operating in Volt-VAr mode. The experimental setup to identify the dynamics of an FSI with GSFs is shown in Fig. 5.

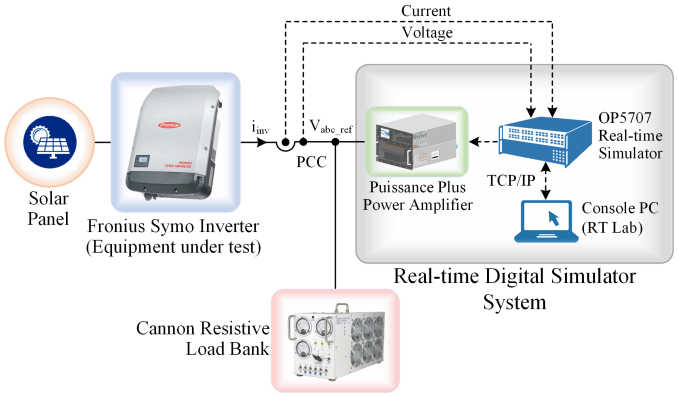

Fig. 5. Experimental setup to determine TF of FSI operated in Volt-VAr mode. The FSI is probed through a power amplifier unit controlled through an Opal-RT RTS.

The OP5707 real-time simulator (RTS) from Opal-RT technology was employed in PHIL. The RTS and power amplifier, in combination with the console PC, were used to emulate grid voltage of varied output magnitude. The voltage amplitude at PCC was perturbed by the power amplifier and the current injected by FSI to the grid was recorded for the complete normal operating range (0.88 p.u. – 1.1 p.u.) to capture the dynamics of Volt-VAr mode. The MATLAB/Simulink model to generate varying voltage amplitude at power amplifier output terminals was designed in the console PC interfaced with OP5707 and was built, compiled, and loaded into OP5707 RTS. Transmission Control Protocol (TCP) and the Internet Protocol (IP) were used to communicate between the console PC and OP5707 RTS. RTS sent the small analog probing signal to the power amplifier input terminals and the amplified probing signal was generated at the output terminals of power amplifier. The DC side of the FSI was powered by a PV system available on the microgrid research lab building at South Dakota State University. A Cannon resistive dump-load was connected at PCC to consume power generated by the PV system and to protect reverse power flow to the power amplifier. The settings of FSI and load are given in Table II.

TABLE II
Load and Fronius Symo Inverter Parameters.

Parameter	Value
Resistive load	1 kW
FSI Rating	10 kW
Q_1, Q_2, Q_3, and Q_4	3.3, 0, 0, and -3.3 kVA resp.
V_L, V_1, V_2, V_3, V_4, and V_H	0.88, 0.92, 0.98, 1.02, 1.07, and 1.1 p.u. resp. [12]

IV. Results and Analysis

The TF of the FSI which operates in Volt-VAr mode is obtained from the SysId toolbox and the results of the GoF obtained by comparing the actual response of an FSI and that from the TF are analyzed in this section.

In PHIL test condition, regions R_1, R_2, R_3, R_4, and R_5 were divided into 3, 7, 3, 5, and 2 ranges based on the voltage parameters (listed in Table II) defined for Volt-VAr mode in the updated IEEE 1547-2018 standard. Middle range data $(r_{12}, r_{24}, r_{32}, r_{43})$ were used to obtain the TF for R_1 up to R_4 regions and range 1 data (r_{51}) was used in region R_5 for all four probing signals. Here, the overall dynamics of the FSI were represented using the second-order TF because the GoF for second-order TF was found to fulfill both accuracy and computational complexity requirements.

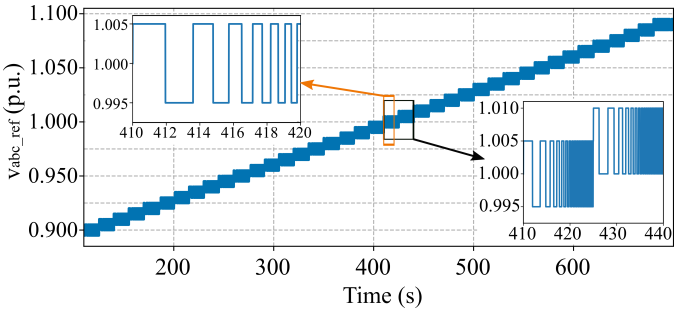

Fig. 6. Logarithmic Sq-Chirp signal used to perturb the voltage at PCC.

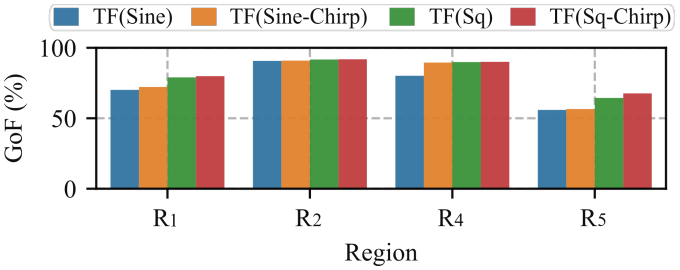

Fig. 7. GoF of two poles and one zero TF model identified from the SysId toolbox. R_3 is not shown as the GSF is not active in that region.

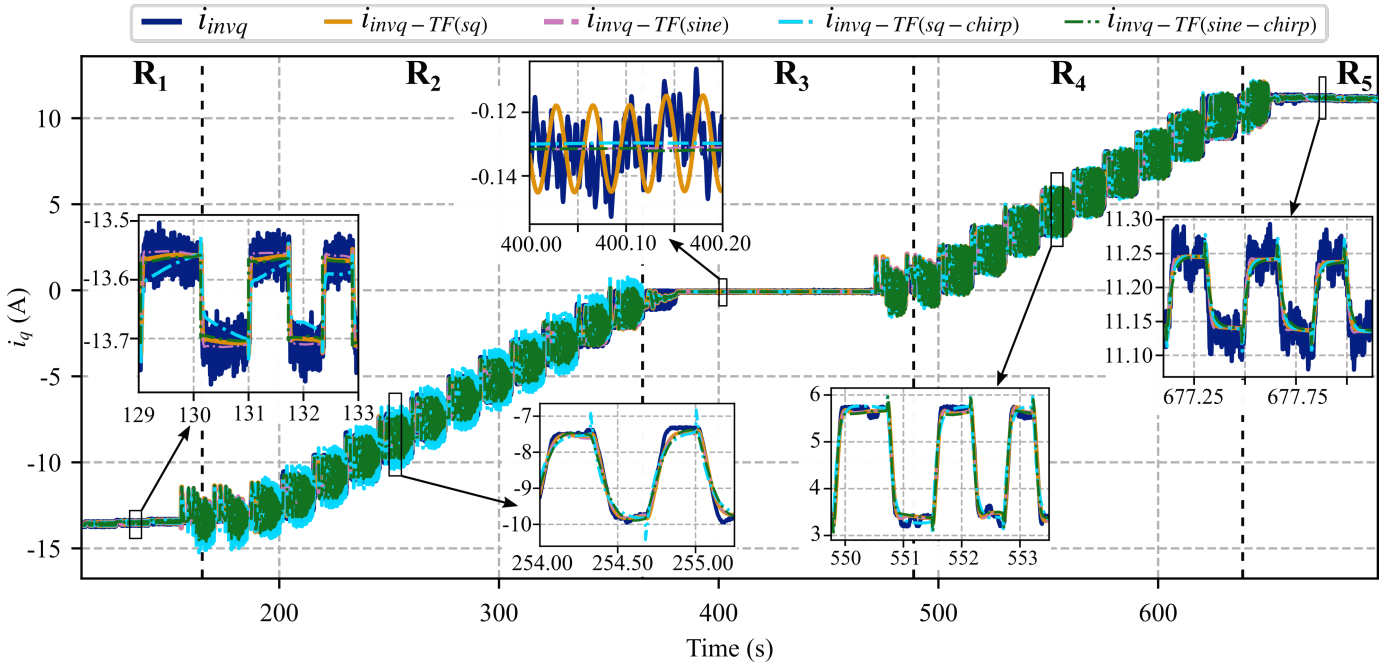

Fig. 8. Response of an FSI when all the TFs from each signal is perturbed by Sq-Chirp.

In contrast to other regions, the Volt-VAr mode is deactivated in the R_3 region, which implies the FSI will not inject/absorb any reactive power to/from the grid, resulting in no significant COTS inverter dynamics. Hence, region R_3 is not considered in the analysis.

Different probing signals were used in Fig. 5 to determine the TFs of FSI operating in Volt-VAr mode. Fig. 6 shows the logarithmic Sq-Chirp signal as a reference input probing signal to change the PCC voltage. TF(Sq), TF(Sine), TF(Sq-Chirp), and TF(Sine-Chirp) were the different TFs obtained from the respective probing signals which include TF for each region (except for R_3) resulting in sixteen TFs. The GoF of TF (2 poles and 1 zero) identified from SysId toolbox available in MATLAB for four probing signals at different regions (except R_3) are shown in Fig. 7. It shows that for all regions, TF obtained from the Sq-Chirp probing signal performs the best. The reason for the high fit percentage with the Sq-Chirp signal is due to the availability of higher frequency components that can capture the dynamics of FSI.

To cross-validate the performance of the probing signal, we excite the derived TFs by all probing signals. Fig. 8 shows the response of an FSI when all the TFs obtained from all probing signal is perturbed by the Sq-Chirp signal. Here, i_{invq} is actual response of an FSI and $i_{invq\_TF(sq)}$, $i_{invq\_TF(sine)}$, $i_{invq\_TF(sq-chirp)}$, and $i_{invq\_TF(sine-chirp)}$ are the output response of the respective TFs. We performed a similar test for all other probing signals but the response is not shown in the paper, overall fit percent is presented. Fig. 9 shows the performance comparison of all the probing signals when fed to all the TFs. It shows that for the regions TF obtained from Sq-Chirp signal has the highest fit percentage. For R_2 and R_4 fit percentage is greater than 95% and R_1 and R_5 has fit percent greater than 75% and 50% respectively. Lower fit in R_1 and R_5 is due to the activation of Volt-VAr mode saturation i.e PV can only inject/absorb constant reactive power regardless of decrease/increase in voltage (below V_1 or above V_4).

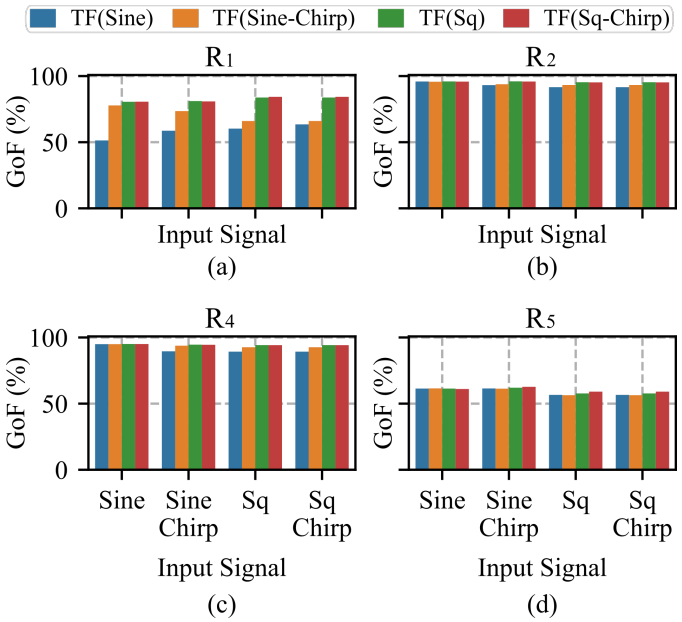

Fig. 9. Performance comparison of all the probing signals when used to perturb all the TFs.

V. Conclusions

A data-driven modeling approach was designed in this research to extract COTS inverter dynamics with GSFs using various probing signals. The SysId toolbox in MATLAB was used to create a dynamic model of a COTS inverter, which was then validated using PHIL under the Volt-VAr GSF. To accurately capture the dynamics of the COTS inverter, predefined regions in piecewise characteristics curve based on the set-point from IEEE 1547-2018 for Volt-VAr mode were used, with each region further partitioned into small ranges. The goodness-of-fit percentage was used to measure the performance of COTS inverter dynamics when the grid voltage was perturbed with each probing signal and described which one would obtain a better model of a COTS inverter. The results show that the logarithmic Sq-chirp signal outperformed in model accuracy based on GoF compared to other probing signals to extract dynamics of COTS inverters. In the future, we intend to explore the effect of solar irradiance in model extraction and validate the model with data from an inverter connected to a feeder that has been operating for a certain number of hours.

Acknowledgments

The authors would like to thank Dr. Atri Bera from Sandia National Laboratories and Niranjan Bhujel from SDSU for their technical review of this paper.

References

[1] IEA. Shares of global electricity generation by source, 2000-2040. [Online]. Available: https://www.iea.org/data-and-statistics/charts/shares-of-global-electricity-generation-by-source-2000-2040

[2] G. Guarderas, A. Frances, R. Asensi, and J. Uceda, "Blackbox large-signal modeling of grid-connected DC-AC electronic power converters," *Energies*, vol. 12, no. 6, 2019.

[3] N. Guruwacharya, N. Bhujel, T. M. Hansen, S. Suryanarayanan, R. Tonkoski, U. Tamrakar, and F. Wilches-Bernal, "Modeling inverters with grid support functions for power system dynamics studies," in *2021 IEEE Power Energy Society Innovative Smart Grid Technologies Conference (ISGT)*, 2021, pp. 1–5.

[4] J. Wang, B. Ji, T. Wu, and J. Chen, "Modeling and analysis of a single phase inverter system with PWM switch model," in *IECON 2014-40th Annual Conference of the IEEE Industrial Electronics Society*. IEEE, 2014, pp. 5115–5119.

[5] B. Hammer, K. Gong, and U. Konigorski, "Modeling and control of inverter-based microgrids," *IFAC-PapersOnLine*, vol. 51, no. 2, pp. 19–24, 2018, 9th Vienna International Conference on Mathematical Modelling.

[6] P. K. Sahu, P. Shaw, and S. Maity, "Modeling and control of grid-connected dc/ac converters for single-phase micro-inverter application," in *2015 Annual IEEE India Conference (INDICON)*, 2015, pp. 1–6.

[7] A. Nagarajan and R. Ayyanar, "Dynamic phasor model of single-phase inverters for analysis and simulation of large power distribution systems," in *2013 4th IEEE International Symposium on Power Electronics for Distributed Generation Systems (PEDG)*, 2013, pp. 1–6.

[8] N. Guruwacharya, N. Bhujel, U. Tamrakar, M. Rauniyar, S. Subedi, S. E. Berg, T. M. Hansen, and R. Tonkoski, "Data-driven power electronic converter modeling for low inertia power system dynamic studies," in *2020 IEEE Power Energy Society General Meeting (PESGM)*, 2020, pp. 1–5.

[9] H. N. Villegas Pico, B. Mather, and G.-S. Seo, "Model identification of inverter nonlinear control dynamics," in *2018 IEEE Electronic Power Grid (eGrid)*, 2018, pp. 1–6.

[10] A. H. Tan and K. R. Godfrey, *Industrial Process Identification—Perturbation Signal Design and Applications*. Springer Nature: Basel, Switzerland, 2019.

[11] R. Javier, F. Zelaya-A, M. Arrieta Paternina, and F. Wilches-Bernal, "Identification of linear power system models using probing signals," in *Proceedings of the 54th Hawaii International Conference on System Sciences*, 2021, p. 3214.

[12] "IEEE Standard for Interconnection and Interoperability of Distributed Energy Resources with Associated Electric Power Systems Interfaces," IEEE Std 1547-2018 (Revision of IEEE Std 1547-2003), Tech. Rep., Apr. 2018.

[13] S. Subedi, N. Guruwacharya, R. Fourney, H. M. Rekabdarkolaee, R. Tonkoski, T. M. Hansen, U. Tamrakar, and P. Cicilio, "Computationally efficient partitioned modeling of inverter dynamics with grid support functions," in *IECON 2021 – 47th Annual Conference of the IEEE Industrial Electronics Society*, 2021, pp. 1–6.

[14] V. Valdivia, A. Lazaro, A. Barrado, P. Zumel, C. Fernandez, and M. Sanz, "Black-box modeling of three-phase voltage source inverters for system-level analysis," *IEEE Transactions on Industrial Electronics*, vol. 59, no. 9, pp. 3648–3662, Sep. 2012.

[15] System identification toolbox. [Online]. Available: https://www.mathworks.com/help/ident/ref/compare.html